KAT8 promotes the resistance of human NSCLC cells to miR-7 intervention via the H4K16/PAX6 axis

Jing Yang
Zunyi Medical University
Xu Zhao
Zunyi Medical University
Dongmei Li
Zunyi Medical University
Lin Tang
Zunyi Medical University
Wen Zheng
Zunyi Medical University
Longqinq Chen
Zunyi Medical University
Jing Chen
Zunyi Medical University
Chao Chen
Zunyi Medical University
Ming Qin
Zunyi Medical University
Mengmeng Guo
Zunyi Medical University
Ya Zhou
Zunyi Medical University
Juanjuan Zhao
Zunyi Medical University
Zhixu He
Zunyi Medical University
Lin Xu (xulinzhouya@163.com)
Zunyi Medical University

Research Article

Keywords: NSCLC, miR-7, Resistance, KAT8, H4K16, PAX6, PI3K/AKT

Posted Date: May 19th, 2022

DOI: https://doi.org/10.21203/rs.3.rs-1663961/v1

Abstract

Background

Accumulating evidence has shown that microRNAs (miRNAs), one of the representative types of noncoding RNAs (ncRNAs), contribute to the development of non-small-cell lung cancer (NSCLC) and act as promising therapeutic targets in NSCLC. However, how to improve the efficiency of miRNA-based gene intervention against NSCLC remains largely unknown.

Methods

A proliferation assay was used to assess the effect of miR-7 intervention on human NSCLC cells. RNA-seq was performed to analyze the global gene expression of miR-7-resistant cells. Mechanistically, coimmunoprecipitation (Co-IP), chromatin immunoprecipitation-polymerase chain reaction (ChIP-PCR) and western blotting were performed.

Results

Under continuous intervention with miR-7, miR-7 levels in human NSCLC cells steadily increased, while its inhibition efficiency gradually decreased. The growth and metastatic capacity of miR-7-resistant human NSCLC cells displaying elevated activation of related signaling pathways were significantly enhanced *in vitro* and *in vivo*. Global gene analysis showed that the expression of paired box 6 (PAX6), a target molecule of miR-7, was obviously increased in these cells. Moreover, PAX6 silencing significantly impaired the aggressive behavior of miR-7-resistant human NSCLC cells, accompanied by decreased transduction of the PI3K/AKT pathway. Mechanistically, the histone acetyltransferase KAT8 regulated PAX6 expression *via* H4K16 acetylation, subsequently resulting in the activation of the PI3K/AKT pathway. Notably, PAX6 silencing significantly improved miR-7 intervention efficiency in human NSCLC cells *in vitro* and *in vivo*. Finally, the relatively higher miR-7 expression was correlated with PAX6 expression in clinical NSCLC tumors.

Conclusion

NSCLC cells acquired resistance to miR-7 intervention, orchestrated by KAT8 regulating PAX6 expression *via* H4K16 acetylation. Specifically, PAX6 silencing significantly improved miR-7 intervention efficiency in human NSCLC cells, thereby providing a feasible approach for miRNA-based intervention in NSCLC.

Introduction

Non-small-cell lung cancer (NSCLC), accounting for 85% of all lung cancer cases, has the highest mortality rate among all solid tumors. Recently, the development and application of targeted gene therapy, represented by tyrosine kinase inhibitors (TKIs) [1], immune checkpoint inhibitors (ICIs) [2] and angiogenesis inhibitors [3], have led to new advances in the efficacy of NSCLC therapies. However, despite the continuous development of driver genes and therapeutic targets for NSCLC, the clinical efficacy of

these interventions on NSCLC, especially advanced NSCLC, is still below 20%, which is related to the complexity of the mechanism of NSCLC development and its resistance to gene therapy drugs, such as EGFR-TKIs [4]. Drug resistance has become the major obstacle in treating NSCLC. Thus, deep investigations of the mechanisms of NSCLC development and drug resistance are urgently needed as is the development of new genetic intervention strategies, which is an important direction in NSCLC research.

MicroRNAs (miRNAs) are single-stranded noncoding RNAs of approximately 19–24 bases that regulate gene expression at the posttranscriptional level, are widely present in various organisms and are involved in important life processes, including embryonic development [5], organ formation [6], cell proliferation [7], differentiation and apoptosis [8]. Numerous studies have shown that miRNAs have important roles in tumor growth and metastasis and potential value in tumor classification [9], diagnosis [10] and prognosis assessment [11]. In terms of tumor gene therapeutic application, miRNAs have the advantages of endogenous presence, small molecular weight, and nonimmunogenicity. Even though some clinical trials involving the treatment of malignancies have been carried out, studies of miRNA-based cancer gene therapy are proceeding slowly, which is partially attributed to the limited delivery efficacy and stability [12, 13]. Therefore, further investigations of the effects and molecular mechanisms of miRNA-based interventions on malignancies, including NSCLC, are urgently needed for the development of novel therapeutic strategies that will ultimately benefit the clinical outcome of cancer patients.

MicroRNA-7 (miR-7), a member of the miRNA family, was first discovered by Lagos-Quintana in 2001. Current evidence shows that miR-7 plays an important regulatory role in the occurrence and development of various diseases, including tumors, cardiovascular diseases, and autoimmune diseases [14, 15]. With regard to NSCLC, accumulating studies have shown that miR-7 can control the growth and metastasis of NSCLC, indicating potential application value in gene therapy against NSCLC [16–18]. However, how and to what extent miR-7-based intervention acts as a therapeutic approach against NSCLC remain largely unknown. In our previous work, we revealed the restricted inhibitory effect of enforced expression of miR-7 on the growth and metastasis of NSCLC *in vivo* [19]. Given that NSCLC usually resists current therapeutic application, we hypothesized that NSCLC may be resistant to miR-7-based intervention, which results in the limited intervention efficacy of miRNA-based gene therapy and hinders the rapid advancement of miRNA applications in cancer gene therapy.

To this end, in the present study, we observed the possible effect of persistent miR-7 intervention on the growth of human NSCLC cells. Our data showed that after multiple interventions with miR-7, the expression level of miR-7 in human NSCLC cells steadily increased, while the inhibition efficiency of miR-7 gradually decreased. Interestingly, the growth and metastatic capacity of human NSCLC cells stably expressing miR-7 were significantly enhanced. Further analysis showed that the expression of paired box 6 (PAX6), a target molecule of miR-7, was obviously increased. Mechanistically, we revealed that the histone acetyltransferase KAT8 regulated PAX6 expression *via* H4K16 acetylation, which further led to aberrant activation of the PI3K/AKT pathway. Of note, PAX6 silencing significantly improved the effect of

miR-7 intervention on human NSCLC cells *in vitro* and *in vivo.* Finally, the relatively higher miR-7 expression was correlated with PAX6 expression in clinical NSCLC tumors. Therefore, this study provides a new research basis for the development of miRNA-based cancer gene biotherapy strategies.

Results

Human NSCLC cells are resistant to miR-7 intervention

To improve the intervention effect of miR-7 on human NSCLC cells, we assessed the possible efficiency of consecutive miR-7 intervention in human NSCLC cells. As expected, we found that in the case of persistent miR-7 intervention, the level of miR-7 in human NSCLC cells increased steadily (Fig. 1A and B). Surprisingly, we noticed that the residual cell number increased rapidly, which was concomitant with the suppression rate of miR-7 on the growth of NSCLC cells gradually decreasing from 70% to less than 20% (Fig. 1C and D). To confirm this phenomenon, we further observed the effect of miR-7 durative overexpression on the growth of NSCLC cells through multiple transfection using a eukaryotic expression vector encoding miR-7 and obtained similar results (Supplementary Fig. 1A-C). Considering the reversibility prevalent in NSCLC resistance to existing therapies, in which NSCLC would be resensitized to therapy after a period of drug withdrawal, we further cultured human NSCLC cells normally for 5 days after consecutive miR-7 intervention and then reassessed the inhibitory effect of miR-7. The data showed that the proliferation of these cells was slowed in the miR-7 group, indicating resensitization to miR-7 intervention (Supplementary Fig. 1G and H).

To facilitate the follow-up study, we then established human NSCLC cells stably expressing miR-7. Real-time PCR results showed that miR-7 was highly expressed in these cells (termed A549/miR-7 and 95D/miR-7 cells) (Fig. 1D and Supplementary Fig. 1D). Importantly, we found that miR-7 intervention could impair the growth of A549/Cont or 95D/Cont cells, which is consistent with our previous findings [19]. However, the growth of human NSCLC A549/miR-7 and 95D/miR-7 cells did not change, displaying resistance to miR-7 intervention. To further observe whether the miR-7 resistance of these cells was specific, we transfected miR-30b, another inhibitor for NSCLC cells, into human NSCLC cells stably expressing miR-7. The data showed that compared with that in the control groups, the growth of all cell populations decreased significantly in the miR-30b-transfected group (Supplementary Fig. 1E and F). Moreover, there were no differences between human NSCLC cells stably expressing miR-7 and their corresponding control cells (Fig. 1E and F). In addition, phalloidin staining results showed that compared with A549/Cont or 95D/Cont cells, A549/miR-7 and 95D/miR-7 cells displayed typical epithelial-mesenchymal transition (EMT) characteristics of looser cell structure and fewer intercellular connections (Fig. 1G and H).

To obtain comprehensive knowledge of the biological characteristics of miR-7-resistant human NSCLC cells, we evaluated the global gene expression of miR-7 stably expressed in human NSCLC cells. The RNA-seq results showed that compared with the 95D/Cont cells, in the 95D/miR-7 cells, 259 genes were upregulated and 251 genes were downregulated (Fig. 1I). Among these genes, multiple genes related to

cell stemness, growth and metastasis were obviously upregulated, while there were no significant differences in apoptosis-related genes (Fig. 1J and K). Moreover, gene set enrichment analysis (GSEA) results showed that there were no significant differences in the expression of RNA sensors, such as TLR3, RIG1 and MDA5, and DNA sensors, such as cGAS/STING, TLR9 and DAI, between the two groups (data not shown). Notably, GO analysis and KEGG analysis further showed that there was elevated transduction activation of multiple signaling pathways, including growth and metastasis, in the 95D/miR-7 cells (Fig. 1L and M). In addition, similar results were obtained in the A549/miR-7 cells and the corresponding control cells (data not shown). Collectively, these findings indicated that human NSCLC cells were specifically resistant to miR-7 intervention, displaying prominent activation of signaling pathways especially related to cell stemness, growth and metastasis.

miR-7-resistant human NSCLC cells show aggressive growth and metastatic capacity

Since proliferation and metastasis-related genes were upregulated in human NSCLC cells stably expressing miR-7, we investigated the growth and metastasis ability of these cells *in vitro* and *in vivo*. Colony formation assay results showed that the colony forming ability of the A549/miR-7 and 95D/miR-7 cells was significantly enhanced compared with that of their corresponding cells (Fig. 2A and B). Consistently, the expression of Ki-67 was markedly upregulated in the A549/miR-7 or 95D/miR-7 cells (Supplementary Fig. 2A). Cell cycle analysis showed that the proportion of cells in G0/G1 and G2/M phase decreased, while the proportion of cells in S phase increased in the A549/miR-7 or 95D/miR-7 cells compared with the A549/Cont or 95D/Cont cells (Fig. 2C and D). In addition, Transwell results showed that the migration and invasion abilities of the A549/miR-7 or 95D/miR-7 cells were observably enhanced compared with those of the A549/Cont or 95D/Cont cells (Supplementary Fig. 2B and C). Notably, the GO and KEGG analyses further showed that there was elevated transduction activation of the MAPK, PI3K/Akt, Ras and Wnt signaling pathways in the 95D/miR-7 cells (Fig. 2E and F, Supplementary Fig. 2D and E). Finally, compared with that in the A549/Cont or 95D/Cont cells, the transduction activation of the PI3K/Akt- and MAPK signaling pathway-related molecules PI3K, p-PI3K, PDK1, Akt, p-Akt, Ras, and p-ERK1/2 in the A549/miR-7 or 95D/miR-7 cells was also upregulated (Fig. 2G and Supplementary Fig. 2F). These data suggested that miR-7-resistant human NSCLC cells exhibited enhanced proliferation and metastatic capacity *in vitro.*

Next, we assessed the proliferation and metastatic ability of these cells *in vivo.* The data showed that compared with those in the A549/Cont group, the tumor volume and weight increased evidently in the A549/miR-7 group (Fig. 2H-J). H&E staining results showed that tumor tissue was more compact in the A549/miR-7 group (Fig. 2K). As expected, the FISH results showed that the expression of miR-7 was significantly upregulated in the tumor mass in the A549/miR-7 group (Fig. 2L). Furthermore, compared with those in the A549/Cont group, the tumor metastasis foci of lung tissue and the lung metastasis index were notably increased in the A549/miR-7 group (Fig. 2M and N). Real-time PCR results showed that compared with those in the A549/Cont group, the expression levels of the cell cycle-related molecules CDK1, CDK2, CDK4, and CDK6 and the metastasis-related molecules MMP2, MMP9 and

CXCR4 were upregulated in tumor tissues in the A549/miR-7 group (Supplementary Fig. 2G and H). WB analysis results further showed that the levels of the PI3K/Akt- and MAPK signaling pathway-related molecules p-PI3k, p-Akt, ERK1/2, p-ERK1/2, and PDK1, the cell cycle-related proteins CDK1 and CCND1, and the metastasis-related proteins vimentin and N-cadherin were significantly upregulated in the A549/miR-7 tumor tissues (Fig. 2O and P). These observations demonstrated that the cell growth and metastasis of miR-7-resistant human NSCLC cells were significantly accelerated *in vitro* and *in vivo.*

PAX6 is upregulated in miR-7-resistant human NSCLC cells

Next, we investigated the possible mechanism of the aggressive behavior of miR-7-resistant human NSCLC cells. Existing evidence has shown that miR-7 controls the carcinogenesis of various cancers, including human NSCLC, by suppressing the expression of its target molecules and that overexpression of these targets can impair the effect of miR-7 on cancer cells [21–23]. Hence, we speculated that the putative target molecules of miR-7 might be responsible for human NSCLC cell resistance to miR-7 intervention. RNA-seq and real-time PCR results preliminarily showed that the expression of PAX6 and YY1, among 8 representative targets of miR-7 in NSCLC, was significantly higher in the A549/miR-7 cells than in the A549/Cont cells (Supplementary Fig. 3A and B). To exclude the bias of selection of putative targets in miR-7-resistant NSCLC cells, we further enriched the upregulated miR-7 target molecules in the A549/miR-7 and 95D/miR-7 cells through Venn analysis. Unexpectedly, the data showed that the expression of PAX6, but not YY1 or other targets, was significantly increased in both cell lines. (Fig. 3A). WB analysis and IF results further showed that compared with that in the A549/Cont cells, the protein level of PAX6 was dramatically upregulated in the A549/miR-7 cells (Fig. 3B-D). Moreover, PAX6 expression was verified in the 95D/miR-7 cells (Supplementary Fig. 4A-E). Consistently, the expression of PAX6 was obviously increased in tumor tissue in the A549/miR-7 cell group (Fig. 3E and F). Finally, to confirm this phenomenon, we observed the expression of PAX6 in human NSCLC cells during consecutive miR-7 intervention. As expected, PAX6 expression increased gradually during multiple interventions with miR-7 in human NSCLC cells (Fig. 3G), which was similar to the miR-7 expression pattern. These results indicated that PAX6 was upregulated in human NSCLC cells, which might contribute to resistance to miR-7 intervention.

PAX6 silencing reduces the resistance of human NSCLC cells to miR-7

Then, to explore whether the upregulation of PAX6 was responsible for the miR-7 resistance of human NSCLC cells, we silenced PAX6 expression using siRNA to analyze the possible effect on the growth and metastatic capacity of miR-7-resistant human NSCLC cells *in vitro* and *in vivo*. Compared with that of the control cells, the growth of the A549/Cont cells decreased in the si-PAX6 transfection group (data not shown), which was consistent with previous reports [23]. Notably, the growth of the A549/miR-7 cells decreased significantly in the si-PAX6 transfection group (Fig. 4A). Scratch assay results showed that compared with the control cells, the migration ability of the A549/miR-7 cells was also obviously impaired in the si-PAX6 group (Fig. 4B). The IF results further showed that the expression of PAX6 and Ki-

67 in the A549/miR-7 cells was significantly decreased (Fig. 4C). Consistent with these findings, the expression levels of PAX6 and the cell cycle-related proteins CDK1, CDK4, and CDK6 were downregulated in the A549/miR-7 cells in the si-PAX6 transfection group. Moreover, the expression levels of p-ERK1/2, p-Akt and PDK1 also decreased dramatically (Fig. 4D). To confirm this phenomenon, we further observed the possible effects of PAX6 silencing on the growth and metastasis of the 95D/miR-7 cells and obtained similar results (Supplementary Fig. 5A-F).

Next, we observed the possible effects of PAX6 silencing on the growth and metastasis of miR-7-resistant human NSCLC cells *in vivo.* Compared with those in the control group, the tumor volume and weight decreased observably in the PAX6-silenced group (Fig. 4E-H). The HE staining results showed that fewer pulmonary metastasis foci were observed in the PAX6-silenced group (Fig. 4I). Immunofluorescence results further showed that compared with that in the control group, the expression of PAX6 was markedly downregulated in tumor tissue in the PAX6-silenced group (Fig. 4J). Furthermore, the lung organ index and tumor metastasis of lung tissue were also reduced (Fig. 4K-L). Notably, consistent with our above findings, the WB analysis results showed that compared with those in the control group, the expression levels of PAX6, the PI3K/Akt- and MAPK signaling pathway-related proteins PI3K, p-Akt, and pERK1/2, and the cell cycle-related proteins CDK1 and CCND1 were significantly decreased in the PAX6-silenced group (Fig. 4M and N). Finally, the metastasis-related protein N-cadherin was also dramatically downregulated in the PAX6-silenced group; conversely, the expression of E-cadherin increased obviously (Fig. 4M and N). These results suggested that PAX6 silencing could weaken the miR-7 resistance of human NSCLC cells.

KAT8 promotes PAX6 upregulation in miR-7-resistant human NSCLC cells

Then, we investigated the probable mechanism of PAX6 upregulation in miR-7-resistant human NSCLC cells. Current evidence shows that miRNAs control their target molecules by binding to the putative sites in the 3'UTR of mRNA. Therefore, we speculated that the sequence variation of miR-7 putative binding sites in the 3'UTR of *PAX6* mRNA might be a reasonable explanation for the increased expression of PAX6 in miR-7-resistant human NSCLC cells. However, RNA sequencing data showed the intact sequences of two binding sites of miR-7 in *PAX6* mRNA in miR-7-resistant human NSCLC cells, indicating that base variation in these binding sites might not contribute to the upregulation of PAX6 (Supplementary Fig. 6). Recently, numerous studies have shown that PAX6 promoter methylation is important for aberrant expression of PAX6 in various malignant diseases [24]. Unexpectedly, our data further showed that there were no significant differences in the promoter methylation levels of *PAX6* between miR-7-resistant cells and their corresponding control cells (Supplementary Fig. 7A-C), suggesting that promoter methylation was also not the main explanation for PAX6 upregulation in miR-7-resistant human NSCLC cells.

Next, considering that histone acetylation, as one of the important regulatory mechanisms in epigenetic regulation, is closely related to gene activation, we hypothesized that the upregulation of PAX6 was

regulated by histone acetylation. First, we assessed the protein acetylation levels and found that the level of total protein acetylation in the A549/miR-7 cells was evidently increased compared with that in the A549/Cont cells (Supplementary Fig. 8A and B). Thus, we further analyzed the expression of the histone acetyltransferases NAT10, SAT1, NAA20, MEAF6, NAT8L, NAA10, KAT8, KAT14, and GNAT1 and the histone deacetylases HDAC1, HDAC2, HDAC3 and HDAC4 in miR-7-resistant human NSCLC cells and their corresponding control cells by RNA-seq and real-time PCR. Interestingly, our data showed that the expression levels of MEAF6, NAA20, KAT8 and KAT14 were markedly increased in miR-7-resistant cells compared with their relevant control cells (Fig. 5A and B). We then performed WB analysis to detect the expression levels of the above proteins in these cells. The data showed that KAT8, among the potential genes, was particularly upregulated in both the A549/miR-7 cells and 95D/miR-7 cells (Fig. 5C and Supplementary Fig. 8C). Most importantly, the real-time PCR results showed that the expression level of KAT8 also steadily increased during multiple interventions of miR-7 in human NSCLC cells (Fig. 5D), displaying a similar expression pattern to that of PAX6.

Next, we further investigated whether elevated expression of KAT8 contributed to PAX6 upregulation in miR-7-resistant human NSCLC cells. The data showed that compared with the control group, KAT8 expression was markedly downregulated in the A549/miR-7 cells in the si-KAT8 transfection group (Fig. 5E). Notably, the mRNA level of PAX6 also decreased dramatically in the si-KAT8 transfection group (Fig. 5F). Furthermore, KAT8 silencing also significantly decelerated the proliferation and migration of the A549/miR-7 cells (Fig. 5G and Supplementary Fig. 9A-E). Moreover, real-time PCR results showed that the expression levels of the cell cycle-dependent kinases CDK1, CDK2, CDK4 and CDK6 and the metastasis-related molecules MMP2, MMP9 and CXCR4 were observably downregulated in the si-KAT8-transfection group (Supplementary Fig. 9F). Consistently, the protein levels of KAT8, p-ERK1/2, p-Akt and p-pPI3K also decreased significantly (Fig. 5H and I). Collectively, these data suggested that the histone acetyltransferase KAT8 mainly contributed to the upregulation of PAX6 and aggressive behaviors of miR-7-resistant human NSCLC cells.

KAT8 regulates PAX6 expression in miR-7-resistant human NSCLC cells via **H4K16 acetylation**

Next, we investigated the underlying mechanism through which KAT8 regulates PAX6 expression. Because KAT8 plays an important role in various malignant diseases by affecting the acetylation level of histone 4 lysine 16 acetylation (H4K16ac) [25], we detected the expression of H4K16ac in miR-7-resistant human cells and found that the expression of H4K16ac was upregulated in the A549/miR-7 cells compared with the A549/Cont cells (Fig. 6A and B). Then, we performed a Co-IP assay to analyze the relationship between KAT8 and H4K16. As expected, our data showed that KAT8 interacted with H4K16ac in the A549/miR-7 cells (Fig. 6C). Importantly, the WB analysis results further showed that the expression levels of KAT8, H4K16ac and PAX6 were significantly higher in the A549/miR-7 cells than in the A549/Cont cells (Fig. 6D and E). Several studies have shown that H4K16 acetylation catalyzed by KAT8 results in the transcriptional expression of multiple genes [26]. Therefore, we further analyzed whether the PAX6 promoter could bind with H4K16ac in the A549/miR-7 cells by ChIP-PCR and ChIP–qPCR assays. Interestingly, our data indicated that H4K16ac could bind to the promoter of PAX6 (Fig. 6F and G). Based

on these results, we further assessed the expression of PAX6 and H4K16ac in the A549/miR-7 cells with KAT8 silencing. WB analysis results showed that the expression of PAX6 and H4K16ac obviously decreased with KAT8 silencing (Fig. 6H). Finally, IF results further showed that KAT8 and H4K16ac had a strong colocalization in miR-7-resistant human NSCLC cells, accompanied by PAX6 expression (Fig. 6I). These data indicated that KAT8 promoted the expression of PAX6 *via* H4K16 acetylation in miR-7-resistant human NSCLC cells.

PAX6 silencing improves the inhibitory effect of miR-7 intervention on NSCLC tumor growth

As our above data showed that PAX6 upregulation contributed to human NSCLC cell resistance to miR-7 intervention, we further investigated whether PAX6 silencing could synergize with the effect of miR-7 intervention on human NSCLC cells. As expected, the data showed that the proliferation of human NSCLC A549 cells was significantly slower in the combined intervention group than in the miR-7-alone intervention group. (Fig. 7A and B). Real-time PCR results showed that compared with the miR-7-alone intervention group, the expression levels of PAX6, the cell cycle-related proteins CDK1, CDK2, CDK4 and CDK6, and the metastasis-related molecules MMP9 and CXCR4 were significantly decreased in the combined intervention group (Fig. 7C). The WB analysis results showed that the expression levels of PDK1, p-Akt, PI3K, p-PI3K, ERK1/2, p-ERK1/2, Ras, Vimentin and PAX6 in the A549 cells were decreased in the combined intervention group compared with the miR-7-alone intervention group (Fig. 7D and E). The IF results further indicated that the expression levels of Ki-67 and PAX6 were obviously reduced in the combined intervention group (Fig. 7F and G). To confirm this phenomenon, we further observed the possible effects of miR-7 combined with PAX6 silencing on the 95D/miR-7 cells and obtained similar results (Supplementary Fig. 10A-E).

Furthermore, we observed the possible effects of miR-7 combined with PAX6 silencing on the the growth and metastasis of human NSCLC cells *in vivo*. Notably, we observed that compared with miR-7 intervention alone, combination intervention could induce the regression of human NSCLC tumors *in vivo*, as evidenced by the gradual decline in the tumor growth curve (Fig. 7H and I). Moreover, the volume and weight of tumors were also obviously decreased in the combination intervention group compared with those in the miR-7-alone intervention group (Fig. 7I and J). H&E staining showed that compared with the miR-7-alone intervention group, the tumor metastasis index of the lung was reduced in the combination therapy group (Fig. 7K and L). The protein levels of PDK1, Ras, p-Akt, PI3K, p-PI3K and PAX6 and the metastasis-related proteins N-cadherin and Vimentin decreased significantly in the tumor mass in the combination intervention group (Fig. 7M and N). These results showed that PAX6 silencing could improve the inhibitory effect of miR-7 intervention on the growth of NSCLC tumors, indicating that this approach might be an effective way to overcome the resistance of human NSCLC cells to miR-7 intervention.

Expression of miR-7 and PAX6 in clinical NSCLC tumors

Although there are a lack of clinical trials of miR-7 gene therapy, we observed a connection between miR-7 and PAX6 expression in clinical NSCLC. Consistent with others and our previous findings [47], miR-7 expression was lower and PAX6 expression was higher in clinical NSCLC tumor tissue (data not shown). To further address whether miR-7 expression prevalence was associated with the clinical characteristics of NSCLC, 21 human NSCLC patients who did not receive antitumor therapy were divided into 2 groups according to the mean value of miR-7 expression: the high miR-7 group (n = 8, average miR-7 level: 0.62 ± 0.26) and the low miR-7 group (n = 13, average miR-7 level: 0.12 ± 0.11). There were no obvious differences in age, tumor stage or TNM classification, while there was a significant difference in tumor size between the high miR-7 group and the low miR-7 group (Fig. 8A and B). Importantly, we found that the expression level of PAX6 was higher in the high miR-7 group than in the low miR-7 group (Fig. 8C). Moreover, similar data were obtained for KAT8 expression (Fig. 8D). Further analysis showed that there was a positive connection between PAX6 and KAT8 expression in NSCLC tumors (Fig. 8E). Consistent with the above findings, we found that, compared with that in adjacent tissue, the expression of PAX6 and KAT8 protein decreased in tumor tissue in the low miR-7 group; however, the expression of PAX6 and KAT8 protein increased in tumor tissue in the high miR-7 group (Fig. 8F and G). Moreover, the expression of both PAX6 and KAT8 in the high miR-7 group was higher than that in the low miR-7 group (Fig. 8F and G). Taken together, these results suggested that a higher miR-7 expression prevalence is connected with PAX6 and KAT8 in clinical tumor tissue, which partially indicates the aggressive status of NSCLC.

Discussion

Over recent decades, positive progress has been achieved in cancer therapy, such as targeted cancer therapy. However, current research has shown that drug resistance has become a hallmark of cancer therapy. The rapidly expanding evidence suggests that noncoding RNAs (ncRNAs), such as miRNAs, long noncoding RNAs (lncRNAs) and PIWI-interacting RNAs (piRNAs), play vital roles in oncogenic processes and drug resistance and represent potential therapeutic targets for cancer, including NSCLC [27]. However, whether there is possible resistance of cancer cells to ncRNA-based therapy, which might impede the development of ncRNA-based cancer gene therapy, has not yet been reported. In this study, we found that human NSCLC cells were resistant to miR-7 treatment, which could be induced by persistent miR-7 intervention. Interestingly, these miR-7-resistant cells were still sensitive to other miRNA interventions, such as miR-30b, indicating that this resistance phenomenon might be inducible and specific. We further revealed that miR-7-resistant human NSCLC cells display not only an EMT phenotype morphologically but also aggressive behavior *in vitro* and *in vivo*. It is well known that some signaling pathways, such as the PI3K/Akt and MAPK signaling pathways, are involved in the drug resistance of various cancers [28–29]. Notably, global gene analysis showed that cell growth- and metastasis-related genes were upregulated and there was aberrant transduction of the PI3K/Akt and MAPK signaling pathways in miR-7-resistant human NSCLC cells. In addition, we noticed that the Wnt signaling pathway associated with tumor cell stemness was significantly increased. These findings suggested that the aggressive behavior of miR-7-resistant human NSCLC cells might be related to aberrant transduction of these related pathways. Therefore, these findings are valuable for successive research on whether human NSCLC cells are

resistant to other distinct ncRNA interventions, especially in clinical trials, which might be critical for the ultimate development of ncRNA-based targeted cancer therapy.

KAT8 (also known as MOF or MYST1) is a major member of the MYST family, which possesses a highly conserved lysine acetyltransferase domain and directly acetylates substrates to participate in a wide range of cellular functions, including cell cycle regulation, the DNA damage response (DDR) and stem cell development [30–32]. Accumulating evidence has shown that KAT8 also plays important roles in not only tumorigenesis, including the proliferation and metastasis of tumor cells, but also the drug resistance of various cancers [33–35]. For instance, Li et al. [36] reported that KAT8 could acetylate H4K16 to regulate cerebral development and syndromic intellectual disability. In this study, we found that the levels of histone acetylation increased obviously in miR-7-resistant human NSCLC cells. Importantly, further analysis showed that the expression of KAT8, but not other HAT family members, was predominantly increased in miR-7-resistant human NSCLC cells. Notably, silencing KAT8 dramatically impaired the aggressive behaviors of miR-7-resistant human NSCLC cells along with reduced transduction of the PI3K/Akt and MAPK signaling pathways. Similarly, recent evidence has shown that KAT8 promotes human NSCLC resistance to multiple therapeutic agents, including cisplatin and EGFR-TKIs [37]. Therefore, our current work further extended existing findings by demonstrating that KAT8 participates in human NSCLC cell resistance to miRNA-based intervention. In addition, regretfully, there were no significant changes in the expression of some well-documented intrinsic nucleic acid sensors in miR-7-resistant human NSCLC cells. Therefore, the exact mechanism of KAT8 expression has not been clearly explored and is still one of our ongoing study projects.

An increasing number of studies have demonstrated that as a transcription factor, PAX6 is not only responsible for maintaining the normal function of essential organs such as the eyes and brain [38] but also plays an indispensable role in the tumorigenesis of lung cancer, breast cancer, and other malignant tumor cells [39–43]. Based on global gene analysis, we revealed that PAX6, as a target molecule of miR-7, was upregulated in miR-7-resistant NSCLC cells. Moreover, PAX6 silencing significantly impaired the aggressive behaviors of miR-7-resistant human NSCLC cells. Consistently, several studies have demonstrated that PAX6 overexpression can reverse the inhibitory effect of miR-7 on multiple cancers, including NSCLC, indicating the important role of PAX6 in miR-7 biological function. Unexpectedly, we found that promoter methylation and sequence variation of miR-7 putative binding sites in the 3'UTR of *PAX6* mRNA might not be the main factors for the upregulation of PAX6 in miR-7-resistant human NSCLC cells. Notably, we revealed that H4K16ac could bind to the promoter of PAX6. Moreover, KAT8 was strongly colocalized with H4K16ac, and KAT8 silencing led to decreased levels of H4K16ac and PAX6 in miR-7-resistant human NSCLC cells. Consistent with the KAT8 expression trend, the expression of PAX6 also increased gradually under persistent miR-7 interventions. Finally, there was a positive connection between the expression of PAX6 and KAT8 in clinical NSCLC patients. Therefore, our data not only demonstrate a novel mechanism by which KAT8 promotes the transcription of PAX6 *via* H4K16ac, thereby contributing to the resistance of human NSCLC to miR-7, but also indicate the potential value of the KAT8/H4K16ac/PAX6 axis in the development of human NSCLC.

Currently, multiple lines of evidence illustrate that combined therapy is an important approach for overcoming the drug resistance of monotherapy, thereby improving the efficiency of cancer treatment. For example, chemotherapy or immunosuppressive agents combined with TKIs have been actively applied in the clinical treatment of NSCLC [44–46]. In our present study, we revealed that the upregulation of PAX6, triggered by KAT8-mediated H4K16ac, was mainly responsible for human NSCLC cell resistance to miR-7 intervention. To preliminarily assess the possible synergistic value of PAX6 in NSCLC-targeted therapy, we observed the effects of miR-7-based gene intervention combined with PAX6 silencing on human NSCLC cells. As expected, PAX6 silencing significantly improved the inhibitory effects of miR-7 on human NSCLC tumor growth and metastasis *in vivo* and *in vitro*, accompanied by altered transduction of the PI3K/Akt and MAPK signaling pathways. Similarly, Wu et al. reported that silencing PAX6 reversed the resistance of NSCLC cells to cisplatin[47]. Finally, we further revealed that the relatively higher expression of miR-7 correlated with PAX6 expression in clinical tumor tissue and partially indicated the aggressive status of NSCLC. Moreover, the expression of both KAT8 and PAX6 was elevated in clinical tumor tissue with higher miR-7 expression. Taken together, our current data suggest the value of a combined strategy for miRNA-7 intervention based on its expression level, which might be helpful for the development of targeted therapies for NSCLC.

Conclusion

In summary, for the first time, we document an unknown phenomenon in which human NSCLC cells gain resistance to miR-7 intervention and provide a feasible approach for miR-7-based intervention in NSCLC. This study revealed that the upregulation of PAX6, facilitated by KAT8-mediated acetylation of H4K16, is mainly responsible for miR-7 resistance in human NSCLC cells (Fig. 8H). Furthermore, we deem that the KAT8/H4K16/PAX6 axis is an ideal target for reversing the miR-7 resistance of human NSCLC. Collectively, these current new findings are of great significance for ncRNA-based gene therapy and surely benefit subsequent in-depth study of the application of combined anticancer strategies.

Methods

Cell culture

Human NSCLC A549 and 95D cells were purchased from Shanghai iCell Bioscience Inc., China. A549 and 95D cells were cultured in RPMI 1640 medium (Gibco, USA) supplemented with 10% fetal bovine serum (FBS, Gibco, USA) and penicillin/streptomycin solution at 37°C with 5% CO_2. All the cells were identified within the past year based on short tandem repeats (STRs) or single nucleotide polymorphisms (SNPs) and were not contaminated with mycoplasma.

siRNA or miRNA mimic transfection

A549 and 95D cells were seeded in a 24-well or 6-well plate and cultured for 24 h. Once the confluence reached 50–60%, PAX6-RNAi or miR-7/miR-30b mimics were transfected by using Lipofectamine® 3000

(Invitrogen, L3000015) following the procedure provided by the manufacturer. After 48 h of transfection, the optical density at 450 nm (OD_{450}) in each well was measured by CCK8 assay. In addition, total RNA and total protein were extracted, and the transcription level of target genes and the related protein expression were detected by quantitative real-time PCR (qPCR) and western blot (WB) analysis, respectively.

Plasmid

The eukaryotic expression vector pcDNA3.1(-)-miR-7 was used in a previous series of work [20]. The vector was identified by enzyme digestion and verified by DNA sequencing for further experiments.

Plasmid transfection and screening of stably transfected cells

A549 and 95D cells were seeded in a 24-well plate and cultured for 24 h. Once the confluence reached approximately 70%, A549 and 95D cells were transfected with pcDNA3.1(-) or pcDNA3.1(-)-miR-7 by using Lipofectamine 3000 reagent (Invitrogen, L3000015) according to the manufacturer's instructions. Forty-eight hours later, the medium was replaced with complete culture medium containing geneticin (G418) at a final concentration of 800 mg/ml or 400 mg/ml. After continuous screening for no less than 15 days, qPCR was performed to detect the RNA levels of miR-7. The transfection efficiency was determined to screen for stably transfected cell lines.

RNA extraction and qPCR

Total RNA in cells and tissues was extracted in accordance with the manual provided with RNAiso Plus (TAKARA, 9108). RNA was quantified and reverse transcribed to cDNA according to the manufacturer's instructions (TAKARA, RR037A). SYBR Green-based real-time qPCR reagents (TAKARA, RR820A) and gene-specific primers were used. The mRNA levels of related genes were quantified using a Bio–Rad CFX96 detection system (Bio–Rad Laboratories). The relative expression levels of genes were calculated by using the comparative threshold cycle (Ct) method with GAPDH as the internal reference.

Western blot analysis

Total protein or nuclear protein in cells or tumor tissues was extracted using lysis buffer (KeyGEN BioTECH, KGP2100) and quantified using the BCA method. Subsequently, the proteins were electrophoresed on 10% sodium dodecyl sulfate–polyacrylamide gel electrophoresis (SDS–PAGE) gels and transferred to polyvinylidene fluoride (PVDF) membranes. The membranes were incubated with 5% skim milk in PBS for 1 hour. The protein bands were then incubated overnight at 4°C with monoclonal antibodies against CDK1 (Abcam, ab201008), CDK4 (CST, #12790), CDK6 (CST, #13331), Cyclin D1 (Abcam, ab16663), AKT (Abcam, ab8805), p-AKT (Abcam, ab38449), ERK1/2 (Abcam, ab184699), p-ERK1/2 (Abcam, ab201015), RAS (Abcam, ab52939), PI3K (Abcam, ab191606), p-PI3K (Abcam, ab182651), KAT8 (Proteintech, 13842-1-AP), H4K16ac (CST, #13534), MEAF6 (Proteintech, 26465-1-AP), NAA (Proteintech, 2015807-1-AP), PAX6 (CST, #60433), N-cadherin (Abcam, ab18203), E-cadherin (Abcam, ab18203), H3 (CST, #4499) and GAPDH (Abcam, 181602). The membranes were washed in PBST and subsequently incubated with an HRP-conjugated anti-rabbit secondary antibody (CST, 7074S). Signals were detected and analyzed using a Bio-Rad ChemiDoc MP Imaging System (Bio-Rad Laboratories). GAPDH was used as the internal reference.

Fluorescence in situ **hybridization (FISH) assay**

FISH was performed using a Dig labeling and detection kit (Roche, 11585614910), and the probes used in this assay were ordered from Denmark EXIQON Co., Ltd. The specific procedure was performed in accordance with the manual provided with the kit. Briefly, tumor tissues were fixed in 4% paraformaldehyde solution to prepare paraffin sections, dewaxed in xylene, rehydrated in an ethanol gradient, subjected to antigen repair using an antigen repair solution (Solarbio, C1037), and hybridized with probes overnight. Then, the cells were observed and photographed under a confocal fluorescence microscope.

Transwell assay

Cells were seeded in Transwell chambers ($8x10^4$/well) after starvation in serum-free RPMI 1640 medium for 24 h. Forty-eight hours later, the cells were fixed with methanol, stained with crystal violet, observed and photographed under a microscope. The number of cells that crossed the membrane was determined.

Establishment of NSCLC models

Five- to eight-week-old female BALB/c nude mice (weight, 18–22 g) were used. All animals were provided by SPF (Beijing) Biotechnology Co., Ltd. and housed in a specific pathogen-free (SPF) class laboratory animal house at Zunyi Medical University. Cells in logarithmic growth phase were collected and resuspended in phosphate-buffered saline (PBS) to form single-cell suspensions. The right axil was inoculated with $1x10^7$ cells. From the date of cell inoculation, tumor growth was closely observed, and tumor growth curves were recorded. After 15 days, nude mice were sacrificed, and the tumors and lungs were removed for subsequent experiments. All animal procedures used in this study were approved by the Animal Ethics Committee of Zunyi Medical University and were performed in accordance with the Guide for the Care and Use of Laboratory Animals.

Plasmid and siRNA transfection in vivo

pcDNA3.1(-)-miR-7 plasmid (50 μg) or PAX6 RNAi (25 μg) was mixed according to the instructions of the *in vivo* transfection kit EntransterTM (Engreen, 18668-11-2). After incubation at room temperature for 15 minutes, the transfection complex (containing 50 μg plasmid) was injected into the distal portion of the tumor once every two days for a total of three times.

Chromatin immunoprecipitation (ChIP)

FISH was performed using a SimpleChIP Plus Sonication Chromatin IP Kit (CST, 56383). The specific procedure was performed in accordance with the manual provided with the kit. Briefly, 16% formaldehyde was used to crosslink $1x10^7$ cells for no more than 10 minutes. After the cell was broken by an ultrasonic fragmentation apparatus, DNA was purified, and the size of the DNA fragment was determined by agarose gel electrophoresis. Then, H4K16ac antibody or IgG was added to the cells and incubated overnight at 4°C (IgG group was used as a negative control). Extracted cell lysates before adding antibodies (input) were also used as a control for target proteins and H3 detection. Then, 300 μl of protein G magnetic beads was added to the antigen antibody complex and incubated at 4°C for 2 hours. Then, the chromatin was eluted and decrosslinked. DNA was purified for the ChIP-PCR assay.

Coimmunoprecipitation (Co-IP)

Co-IP assays were performed using a Pierce Co-Immunoprecipitation (Co-IP) Kit (Thermo Scientific™, 01060543) according to the manufacturer's instructions. The IgG group was used as a negative control. Cell lysates extracted prior to antibody addition (input) were also used as controls for target protein and

H3 detection. Subsequently, the possible proteins that bind to KAT8 were identified by mass spectrometry and verified by WB analysis.

Cell cycle analysis

The distribution of A549/miR-7 and 95D/miR-7 cells in the cell cycle phases was analyzed by measuring DNA content using a flow cytometer (Gallio, BECKMAN). This assay was performed with a DNA Content Quantitation Assay kit (Solarbio, CA1510) according to the manufacturer's instructions.

Patients and tissue samples

A total of 21 Chinese patients who were diagnosed with lung cancer between 2021 and 2022 were included in the present study. Clinical and pathological information, including age, sex, tumor type and disease stage, was collected. Paraffin blocks and fresh-frozen tumor specimens of tumor samples from all 21 patients were prepared. In addition, 8 samples from normal tissues adjacent to the tumors were also collected. All the patients were followed up until April 2022. This study was approved by the Ethics Committee of the Second Hospital of Zunyi Medical University (Guizhou, China), and written informed consent was obtained from all the participants.

Cell counting kit-8 (CCK8) assay

CCK8 reagent (MCE, HY-K0301) in fresh complete medium (1:9) was added to transfected human NSCLC A549 and 95D cells seeded in 96-well plates and incubated for 2 hours. The optical density at 450 nm (OD_{450}) in each well was measured in the dark with a microplate reader, and an absorbance curve was generated.

Statistical analysis

Statistical analysis was performed using GraphPad Prism 5 software. One-way ANOVA followed by Bonferroni's *post hoc* test was applied for multiple comparisons, and Student's t test was used when two conditions were compared. A two-tailed $p < 0.05$ was considered statistically significant. All data are shown as the mean ± standard error of the mean (SEM). Survival was evaluated by the Kaplan–Meier method.

Abbreviations

NSCLC, Non-small-cell lung cancer; TKIs, Tyrosine kinase inhibitors; miRNA, MicroRNA; ICI, Immune checkpoint inhibitor; miR-7, MicroRNA-7; FCM, Flow cytometry; RNAi, RNA interference; ChIP, Chromatin immunoprecipitation; qPCR, Real-time PCR; Co-IP, Coimmunoprecipitation; FISH, Fluorescence in situ hybridization; WB, Western blot; p-AKT, Phosphorylated AKT; p-PI3K, Phosphorylated PI3K; p-ERK1/2, Phosphorylated ERK1/2; Ki67, Cell proliferation nuclear antigen; PAX6, Paired box 6; KAT8, lysine acetyltransferase; H4K16ac, H4K16 acetylation; G418, Geneticin; YY1, YinYang 1; ncRNAs, Noncoding RNAs; lncRNAs, Long noncoding RNAs; piRNAs, PIWI-interacting RNAs

Declarations

Ethics approval and consent to participate

The experimental procedures were approved by the Zunyi Medical University Laboratory Animal Care and Use Committee (permit number: SYXK-2019-004).

Consent for publication

All listed authors have approved the manuscript before submission, including the names and order of authors.

Availability of supporting data and materials

The data analyzed during this study are available from the corresponding author on reasonable request.

Competing interests

The authors declare no competing interests.

Funding

This manuscript was supported by the National Natural Science Foundation of China (32160178, 81960509), the Program for High Level Innovative Talents in Guizhou Province (QKH-RC-2016-4031), the Program for Excellent Young Talents of Zunyi Medical University (15ZY-001), the Project of Guizhou Provincial Department of Science and Technology (QKHZC-2020-4Y156), and the Guizhou Province Graduate Research Fund (YJSCXJH-2020-093), the Program for Science and Technology Joint Fund Project in Zunyi Science and Technology Bureau and Zunyi Medical University (ZSKH-HZ-2021-276), Guizhou Province Science and Technology Planning Project (QKPTRC-2019-052),Collaborative Innovation Center of Chinese Ministry of Education (2020-39), Science and technology Fund project of Guizhou Provincial Health Commission.

Authors' contributions

J.Y., X.Z., and L.X. designed the study. X.Z., D.L., L.T., W.Z., L.C., J.C., C.C., M.Q, M.G, and Y.Z. performed the experiments. J.Y., X.Z., J.Z., M.Q. and L.T. analyzed the data. J.Y. and L.X. wrote the manuscript with contribution from all coauthors.

Acknowledgements

We thank AJE (www.aje.cn.com) for its linguistic assistance and scientific consultation during the preparation of this manuscript.

References

1. Sequist L, Yang J, Yamamoto N, O'Byrne K, Hirsh V, Mok T, et al. Phase III study of afatinib or cisplatin plus pemetrexed in patients with metastatic lung adenocarcinoma with EGFR mutations. J Clin Oncol. 2013;31(27):3327-34.
2. Cascone T, William W, Weissferdt A, Leung CH, Lin HY, Pataer A, et al. Neoadjuvant nivolumab or nivolumab plus ipilimumab in operable non-small cell lung cancer: the phase 2 randomized NEOSTAR trial. Nat Med. 2021;27(3):504-14.
3. Zhou M, Lu W, Li B, Liu X, Li A. TARBP2 promotes tumor angiogenesis and metastasis by destabilizing antiangiogenic factor mRNAs. Cancer Sci. 2021;112(3):1289-99.
4. Fu Y, Zhang Y, Lei Z, Liu T, Cai T, Wang A, et al. Abnormally activated OPN/integrin αVβ3/FAK signalling is responsible for EGFR-TKI resistance in EGFR mutant non-small-cell lung cancer. J Hematol Oncol. 2020;13(1):169.
5. Saliminejad K, Khorram Khorshid H, Soleymani Fard S, Ghaffari SH. An overview of microRNAs: Biology, functions, therapeutics, and analysis methods. J Cell Physiol. 2019;234(5):5451-65.
6. Shi Y, Jin Y. MicroRNA in cell differentiation and development. Sci China C Life Sci. 2009;52(3):205-11.
7. Prieto-Colomina A, Fernández V, Chinnappa K, Borrell V. MiRNAs in early brain development and pediatric cancer: At the intersection between healthy and diseased embryonic development. Bioessays. 2021;43(7):e2100073.
8. Takasaki S. Roles of microRNAs in cancers and development. Methods Mol Biol. 2015;1218:375-413.
9. Liu K, Chen H, You Q, Wang F, Wang S, Zhang S, et al. miR-145 inhibits human non-small-cell lung cancer growth by dual-targeting RIOK2 and NOB1. Int J Oncol. 2018;53(1):257-265.
10. Zhao B, Han H, Chen J, Zhang Z, Li S, Fang F, et al. MicroRNA let-7c inhibits migration and invasion of human non-small cell lung cancer by targeting ITGB3 and MAP4K3. Cancer Lett. 2014;342(1):43-51.
11. Xu S, Shi L. High expression of miR-155 and miR-21 in the recurrence or metastasis of non-small cell lung cancer. Oncol Lett. 2019;18(1):758-763.
12. Morrissey D, Lockridge J, Shaw L, Blanchard K, Jensen K, Breen W, et al. Potent and persistent in vivo anti-HBV activity of chemically modified siRNAs. Nat Biotechnol. 2005;23(8):1002-7.
13. Li Z, Rana T. Therapeutic targeting of microRNAs: current status and future challenges. Nat Rev Drug Discov. 2014;13(8):622-38.
14. Zhang J, Zhao M, Yan R, Liu J, Maddila S, Junn E, et al. MicroRNA-7 Protects Against Neurodegeneration Induced by α-Synuclein Preformed Fibrils in the Mouse Brain. Neurotherapeutics. 2021;18(4):2529-40.
15. Zhao J, Chu F, Xu H, Guo M, Shan S, Zhen W, et al. C/EBPα/miR-7 Controls CD4 T-Cell Activation and Function and Orchestrates Experimental Autoimmune Hepatitis in Mice. Hepatology (Baltimore, Md). 2021;74(1):379-96.

16. Li Q, Wu X, Guo L, Shi J, Li J. MicroRNA-7-5p induces cell growth inhibition, cell cycle arrest and apoptosis by targeting PAK2 in non-small cell lung cancer. FEBS open bio. 2019;9(11):1983-93.
17. Xiao H. MiR-7-5p suppresses tumor metastasis of non-small cell lung cancer by targeting NOVA2. Cell Mol Biol Lett. 2019;24:60.
18. Chen R, Qian Z, Xu X, Zhang C, Niu Y, Wang Z, et al. Exosomes-transmitted miR-7 reverses gefitinib resistance by targeting YAP in non-small-cell lung cancer. Pharmacol Res. 2021;165:105442.
19. Lei L, Chen C, Zhao J, Wang H, Guo M, Zhou Y, et al. Targeted Expression of miR-7 Operated by TTF-1 Promoter Inhibited the Growth of Human Lung Cancer through the NDUFA4 Pathway. Mol Ther Nucleic Acids. 2017;6:183-97.
20. Xu L, Wen Z, Zhou Y, Liu Z, Li Q, Fei G, et al. MicroRNA-7-regulated TLR9 signaling-enhanced growth and metastatic potential of human lung cancer cells by altering the phosphoinositide-3-kinase, regulatory subunit 3/Akt pathway. Mol Biol Cell. 2013; 24(1).
21. Su T, Huang S, Zhang Y, Guo Y, Zhang S, Guan J, et al. miR-7/TGF- β2 axis sustains acidic tumor microenvironment-induced lung cancer metastasis. Acta Pharm Sin B. 2022;12(2).
22. Cao Q, Mao ZD, Shi YJ, Chen Y, Sun Y, Zhang Q, et al. MicroRNA-7 inhibits cell proliferation, migration and invasion in human non-small cell lung cancer cells by targeting FAK through ERK/MAPK signaling pathway.Oncotarget. 2016;7(47).
23. Luo J, Li H, Zhang C. MicroRNA-7 inhibits the malignant phenotypes of non-small cell lung cancer in vitro by targeting Pax6. Mol Med Rep. 2015;12(4).
24. Urrutia G, Laurito S, Campoy E, Nasif D, Branham MT, Roqué M. PAX6 Promoter Methylation Correlates with MDA-MB-231 Cell Migration, and Expression of MMP2 and MMP9. Asian Pac J Cancer Prev. 2018;19(10).
25. Radzisheuskaya A, Shliaha PV, Grinev VV, Shlyueva D, Damhofer H, Koche R, et al. Complex-dependent histone acetyltransferase activity of KAT8 determines its role in transcription and cellular homeostasis. Mol Cell. 2021;81(8)
26. Zhong J, Ji L, Chen H, Li X, Zhang J, Wang X, et al. Acetylation of hMOF Modulates H4K16ac to Regulate DNA Repair Genes in Response to Oxidative Stress. Int J Biol Sci. 2017;13(7).
27. Diener C, Keller A, Meese E. Emerging concepts of miRNA therapeutics: from cells to clinic. Trends Genet 2022; 15.
28. Zhang Y, Kwok-Shing Ng P, Kucherlapati M, Chen F, Liu Y, Tsang YH, et al. A Pan-Cancer Proteogenomic Atlas of PI3K/AKT/mTOR Pathway Alterations. Cancer Cell. 2017; 31(6):820-832.e3.
29. Zhang Y, Bao C, Mu Q, Chen J, Wang J, Mi Y, et al. Reversal of cisplatin resistance by inhibiting PI3K/Akt signal pathway in human lung cancer cells. Neoplasma. 2016;63(3):362-70.
30. Rea S, Xouri G, Akhtar A. Males absent on the first (MOF): from flies to humans. Oncogene. 2007;26(37).
31. Sheikh BN, Bechtel-Walz W, Lucci J, Karpiuk O, Hild I, Hartleben B, et al. MOF maintains transcriptional programs regulating cellular stress response. Oncogene. 2016;35(21).

32. Singh M, Bacolla A, Chaudhary S, Hunt CR, Pandita S, Chauhan R, et al. Histone Acetyltransferase MOF Orchestrates Outcomes at the Crossroad of Oncogenesis, DNA Damage Response, Proliferation, and Stem Cell Development. Mol Cell Biol. 2020;40(18).
33. Dong Z, Zou J, Li J, Pang Y, Liu Y, Deng C, et al. MYST1/KAT8 contributes to tumor progression by activating EGFR signaling in glioblastoma cells. Cancer Med. 2019;8(18).
34. Poté N, Cros J, Laouirem S, Raffenne J, Negrão M, Albuquerque M, et al. The histone acetyltransferase hMOF promotes vascular invasion in hepatocellular carcinoma. Liver Int. 2020;40(4).
35. Hajji N, Wallenborg K, Vlachos P, Füllgrabe J, Hermanson O, Joseph B. Opposing effects of hMOF and SIRT1 on H4K16 acetylation and the sensitivity to the topoisomerase II inhibitor etoposide. Oncogene 2010;29(15).
36. Li L, Ghorbani M, Weisz-Hubshman M, Rousseau J, Thiffault I, Schnur RE, et al. Lysine acetyltransferase 8 is involved in cerebral development and syndromic intellectual disability. J Clin Invest. 2020;130(3).
37. Singh DK, Pandita RK, Singh M, Chakraborty S, Hambarde S, Ramnarain D, et al. MOF Suppresses Replication Stress and Contributes to Resolution of Stalled Replication Forks. Mol Cell Biol 2018;38(6).
38. Jin Y, Zhang B, Lu J, Song Y, Wang W, Zhang W, et al. Long noncoding RNA PM maintains cerebellar synaptic integrity and Cbln1 activation via Pax6/Mll1-mediated H3K4me3. PLoS Biol. 2021;19(6):e3001297.
39. Zhang X, Yang X, Wang J, Liang T, Gu Y, Yang D. Down-regulation of PAX6 by promoter methylation is associated with poor prognosis in non small cell lung cancer. Int J Clin Exp Pathol . 2015;8(9):11452-7.
40. Kiselev Y, Andersen S, Johannessen C, Fjukstad B, Standahl Olsen K, Stenvold H, et al. Transcription factor PAX6 as a novel prognostic factor and putative tumour suppressor in non-small cell lung cancer. Sci Rep. 2018;8(1):5059.
41. Zhang X, Xu J, Zhang H, Sun J, Li N, Huang X. MicroRNA-758 acts as a tumor inhibitor in colorectal cancer through targeting PAX6 and regulating PI3K/AKT pathway. Oncol Lett. 2020;19(6):3923-30.
42. Xu Q, Liu K. MiR-369-3p inhibits tumorigenesis of hepatocellular carcinoma by binding to PAX6. J Biol Regul Homeost Agents. 2020;34(3):917-926.
43. Zou Q, Yi W, Huang J, Fu F, Chen G, Zhong D. MicroRNA-375 targets PAX6 and inhibits the viability, migration and invasion of human breast cancer MCF-7 cells. Exp Ther Med. 2021;22(4):1169.
44. Pérol M, Felip E, Dafni U, Polito L, Pal N, Tsourti Z, et al. Effectiveness of PD-(L)1 inhibitors alone or in combination with platinum-doublet chemotherapy in first-line (1L) non-squamous non-small-cell lung cancer (Nsq-NSCLC) with PD-L1-high expression using real-world data. Ann Oncol. 2022;
45. Peng DH, Rodriguez BL, Diao L, Gaudreau PO, Padhye A, Konen JM, et al. Th17 cells contribute to combination MEK inhibitor and anti-PD-L1 therapy resistance in KRAS/p53 mutant lung cancers. Nat Commun. 2021;12(1).

46. Hayashi H, Chiba Y, Sakai K, Fujita T, Yoshioka H, Sakai D, et al. A Randomized Phase II Study Comparing Nivolumab With Carboplatin-Pemetrexed for Patients With EGFR Mutation-Positive Nonsquamous Non-Small-Cell Lung Cancer Who Acquire Resistance to Tyrosine Kinase Inhibitors Not Due to a Secondary T790M Mutation: Rationale and Protocol Design for the WJOG8515L Study. Clin Lung Cancer. 2017;18(6).
47. Wu D, Zhang T, Liu Y, Deng SH, Han R, Liu T, et al. The PAX6-ZEB2 axis promotes metastasis and cisplatin resistance in non-small cell lung cancer through PI3K/AKT signaling. Cell Death Dis. 2019;10(5):349.

Figures

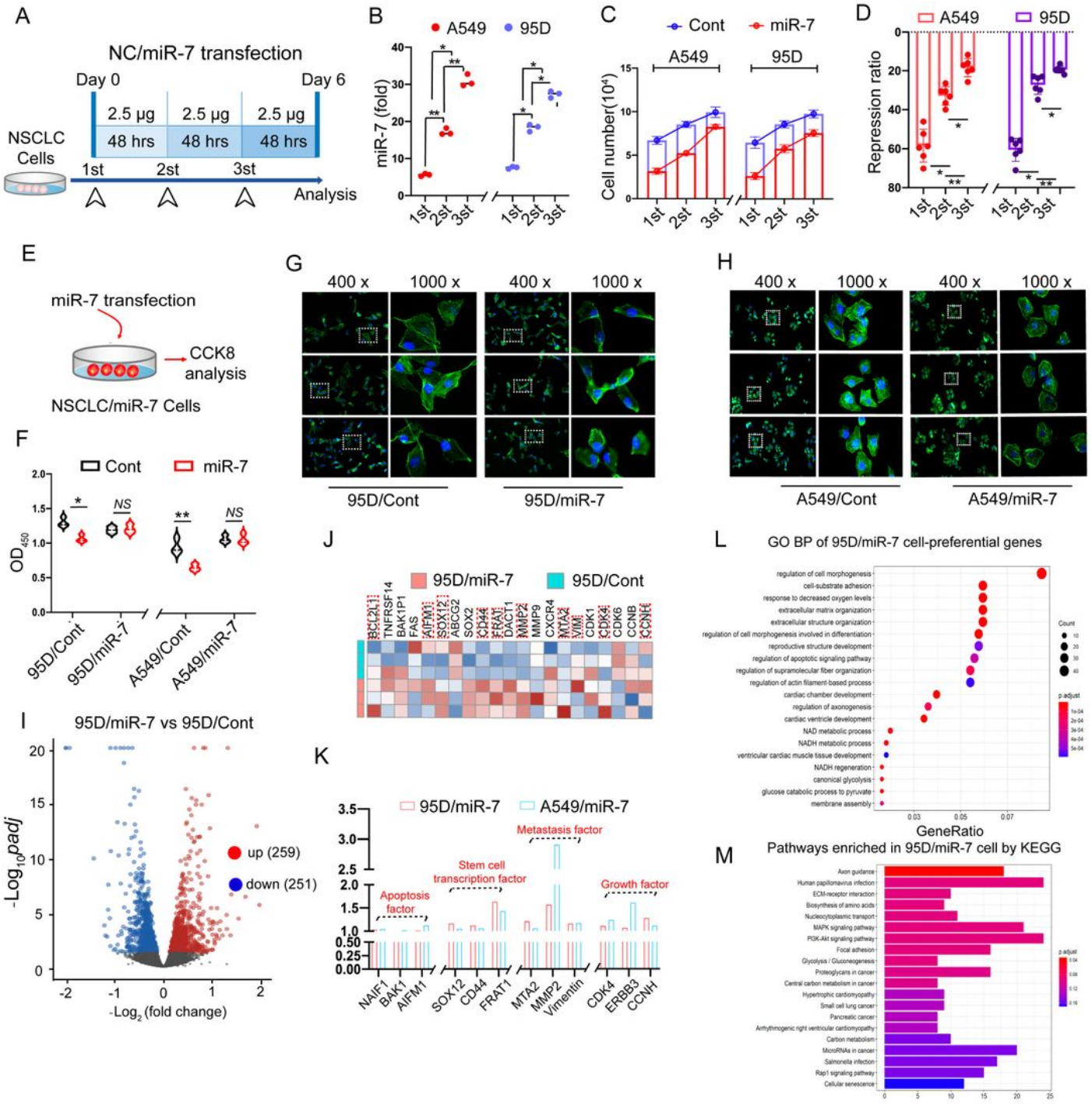

Figure 1

Figure 1

Human NSCLC cells are resistant to miR-7 intervention.

(A) Schematic diagram. Human NSCLC cells were transiently transfected with miR-7 mimics (2.5 μg) in 24-well plates using Lipofectamine 3000 reagent *in vitro*, once every two days, three times in total. **(B)** The expression of miR-7 in (A) was detected by real-time PCR. **(C)** The cell number of (A) was calculated.

(D) The repression ratio of miR-7 in (A) was quantitated by CCK8 assay. **(E)** Schematic diagram. Human NSCLC cells were transiently transfected with the p-Cont/p-miR-7 vector (2.5 μg) in 24-well plates using Lipofectamine 3000 reagent *in vitro* and screened by G418 for 14 days. Then, these cells were transiently transfected with miR-7 mimics and the corresponding control (2.5 μg) in 24-well plates using Lipofectamine 3000 reagent *in vitro*. **(F)** Forty-eight hours later, the proliferation of (E) was detected by CCK8 assay. **(G-H)** The cytoskeleton of these cells was detected by immunofluorescence (400×, 1000×). **(I)** Volcano map showing the differentially expressed genes between the 95D/miR-7 cells and 95D/Cont cells. **(J-K)** The biological characteristics and fold changes in gene expression differences between the 95D/miR-7 cells and 95D/Cont cells were analyzed by RNA-seq. **(L-M)** GO analysis and KEGG enrichment were used to analyze the biological changes and signaling pathways of the 95D/miR-7 cells and 95D/Cont cells. Representative data from three independent experiments are shown. *NS, no significance*, *$p<0.05$, **$p<0.01$.*

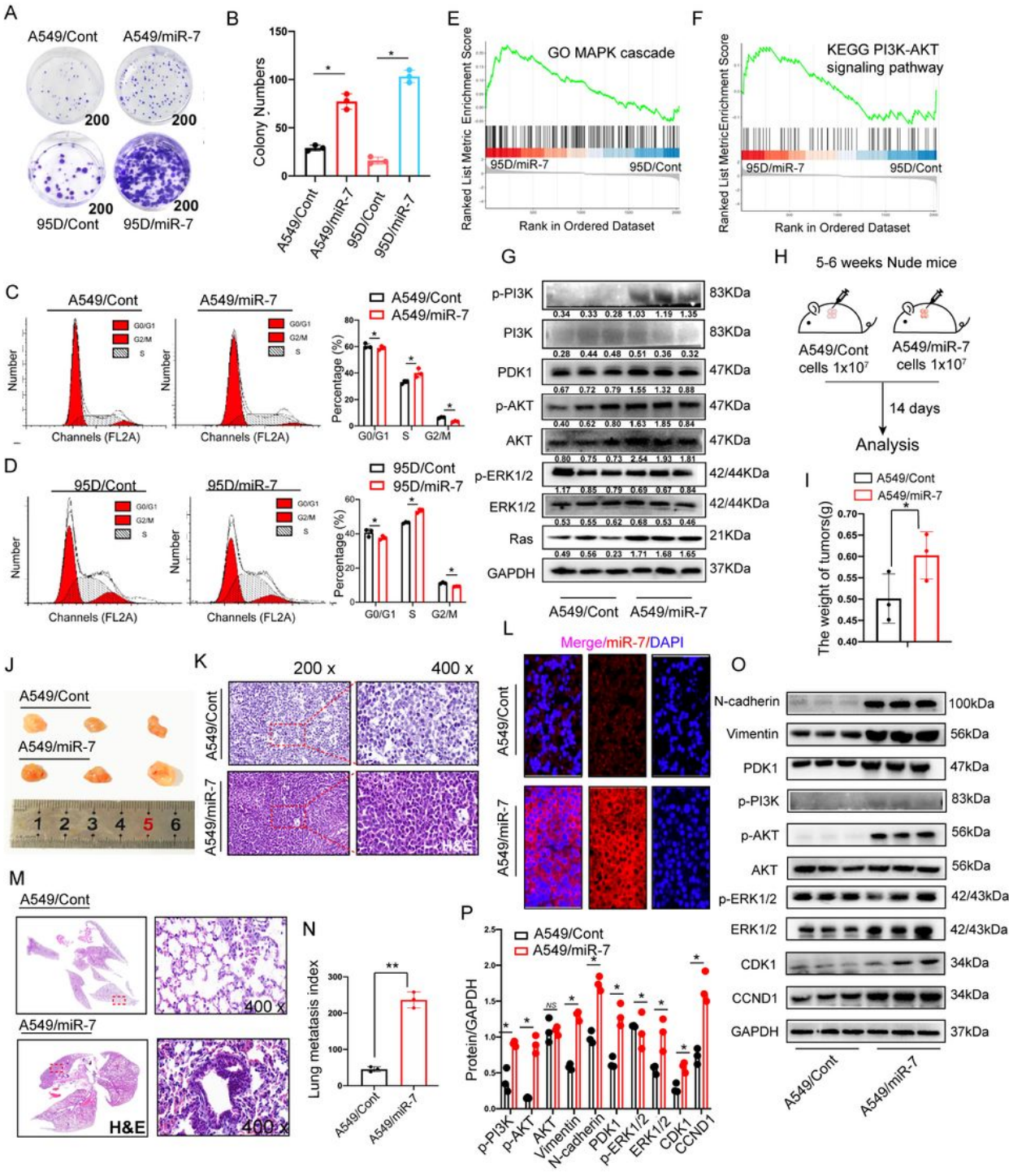

Figure 2

Figure 2

The growth and migration of miR-7-resistant human NSCLC cells *in vitro* and *in vivo*.

(A-B) The proliferation of miR-7-resistant human NSCLC cells and their corresponding control cells was detected by a colony formation assay and calculated. **(C-D)** The cell cycle distribution of these cells was detected by FACS. **(E-F)** GO analysis and KEGG enrichment were used to analyze the MAPK and PI3K/Akt

signaling pathways of 95D/miR-7 cells and 95D/Cont cells. **(G)** The expression levels of the PI3K/Akt- and MAPK-related molecules PI3K, p-PI3K, AKT, p-AKT, ERK1/2, p-ERK1/2, Ras and PDK1 in the A549/miR-7 cells and A549/Cont cells were analyzed by western blotting and calculated. **(H)** Schematic diagram. Subcutaneous injection of A549/Cont and A549/miR-7 cells ($1X10^7$) into the right flanks of Balb/c nude mice. After 15 days, tumor and lung tissues were harvested. **(I)** Tumor weight. **(J)** Tumor size and **(K)** representative hematoxylin and eosin-stained tumor tissue in (H) (200×, 400×). **(L)** The expression of miR-7 in tumor tissues was analyzed by FISH. **(M-N)** The histopathology of lung tissues in (A) was observed (200×, 400×). The metastatic index was calculated. **(O-P)** The expression levels of the PI3K/Akt- and MAPK signaling pathway-related molecules PDK1, p-PI3K, AKT, p-AKT, ERK1/2 and p-ERK1/2, the cell cycle-dependent molecules CDK1 and CCND1, and the metastasis-related molecules N-cadherin and vimentin in tumor tissues of (A) were detected by western blotting and calculated. Representative data from three independent experiments are shown. *NS, no significance, **p<0.01, *p<0.05.*

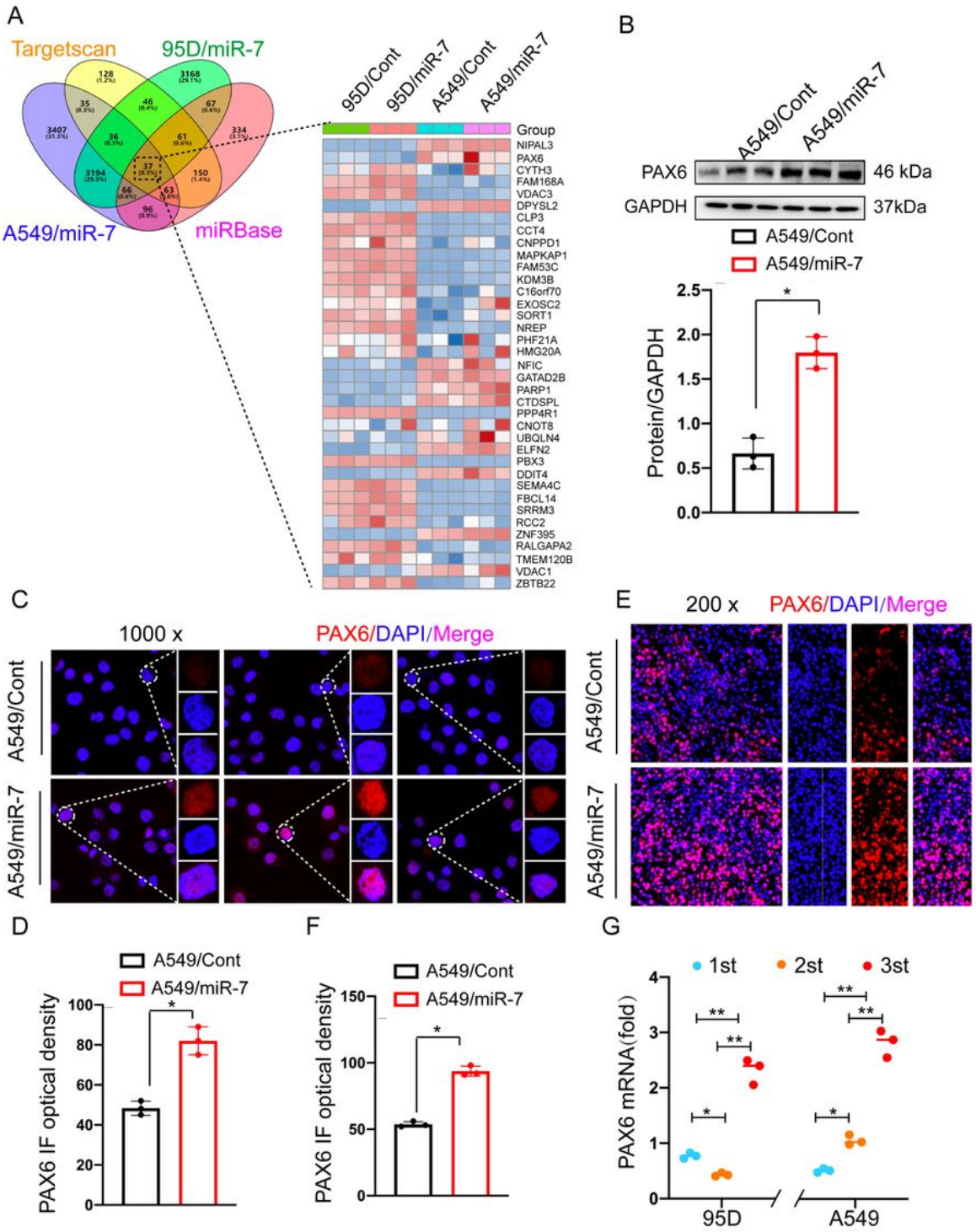

Figure 3

Figure 3

PAX6 is upregulated in miR-7-resistant human NSCLC cells.

(A) An RNA-seq assay was performed in miR-7-resistant human NSCLC cells. Wayne analysis of miR-7 target genes using miRBase and TargetScan. **(B)** The protein level of PAX6 in A549/miR-7 cells and A549/Cont cells was analyzed by western blotting and calculated. **(C-F)** The expression of PAX6 in

A549/miR-7 and A549/Cont cells was analyzed by immunofluorescence and quantitated *in vitro* and *in vivo* **(E** and **F)**. **(G)** The expression of PAX6 in human NSCLC A549 cells and 95D cells under continuous intervention with miR-7 was detected by real-time PCR and calculated. Representative data from three independent experiments are shown. **p<0.05, **p<0.01.*

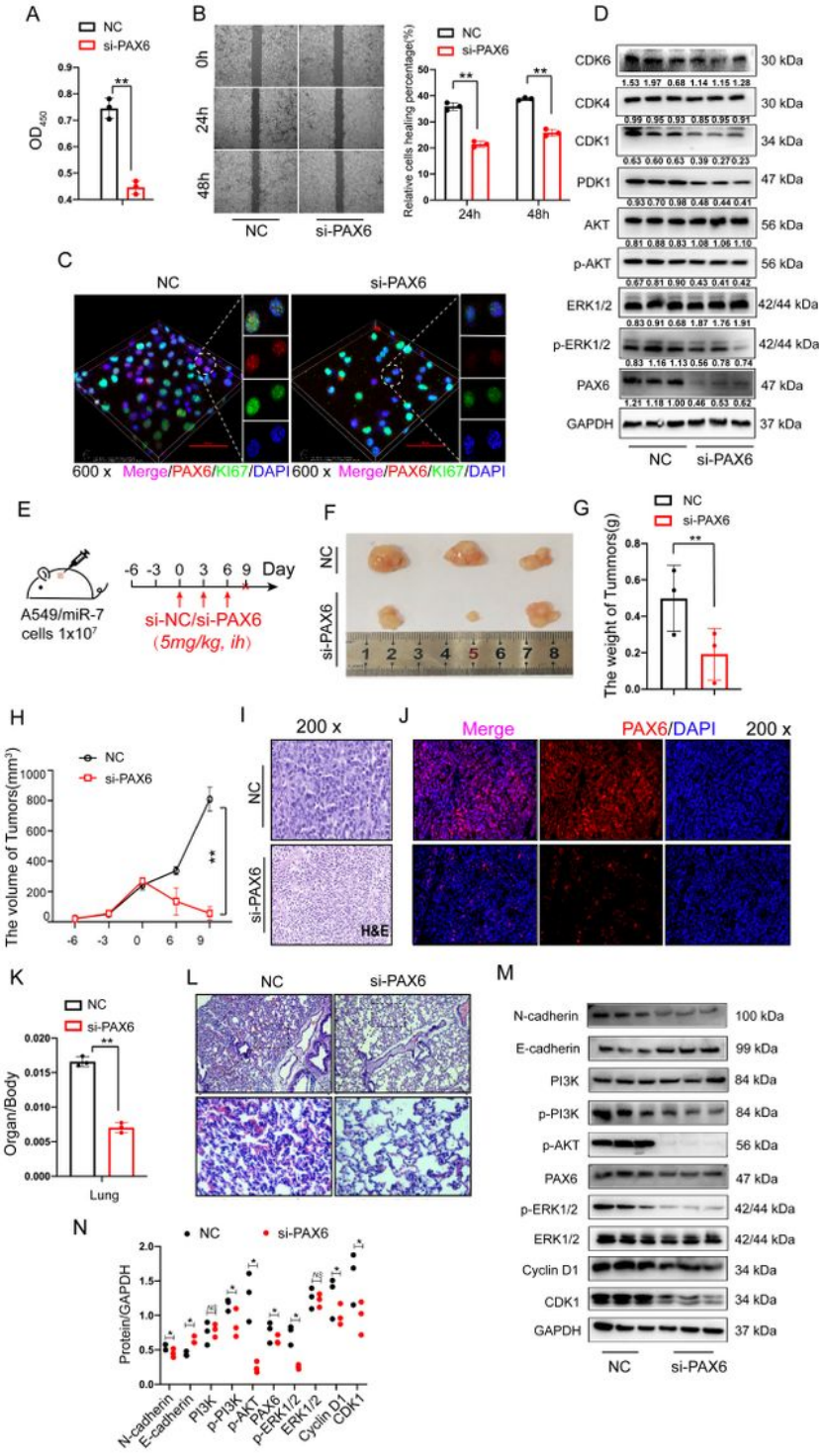

Figure 4

Figure 4

PAX6 silencing impairs the aggressive behavior of miR-7-resistant human NSCLC cells *in vitro and in vivo.*

(A) A549/miR-7 cells were transiently transfected with PAX6 siRNA and control siRNA (2.5 nM) in 24-well plates using Lipofectamine 3000 reagent *in vitro*. Forty-eight hours later, the proliferation of A549/miR-7 cells was assessed by CCK8 assay. **(B)** The migration of (A) was performed by scratch assay and calculated. **(C)** Immunofluorescence was performed to detect the expression of PAX6 and Ki-67 in (A) (×600). **(D)** The expression levels of PAX6, the cell cycle molecules CDK1, CDK4 and CDK6, and the PI3K/AKT- and MAPK pathway-related molecules AKT, p-AKT, ERK1/2, p-ERK1/2 and PDK1 in (A) were detected by western blotting and calculated. **(E)** Schematic diagram. Subcutaneous injection of A549/Cont and A549/miR-7 cells ($1X10^7$) into the right flanks of Balb/c nude mice. After 7 days, the mice were injected with PAX6 siRNA and control siRNA (25 nM) every two days for a total of 3 injections. Tumor growth was monitored every three days to generate the growth curve. On day 15, tumor and lung tissues were harvested. **(F)** Tumor volume. **(G)** Tumor weight. **(H)** Tumor growth curve. **(I)** The representative hematoxylin and eosin-stained tumor tissue in (E) (200×). **(J)** PAX6 expression in tumor tissue was detected by immunofluorescence (200×). **(K)** The organ index of lung tissues in (E) was calculated. **(L)** The pathological changes in the lung tissues in (E) were analyzed by HE staining and quantified. **(M-N)** The expression levels of PAX6, the PI3K/Akt- and MAPK signaling pathway-related molecules PI3K, p-PI3K, p-AKT, ERK1/2 and p-ERK1/2, the cell cycle-dependent molecules CDK1 and CCND1, and the metastasis-related molecules N-cadherin and vimentin in (E) were detected by western blotting and calculated. Representative data from three independent experiments are shown. *NS, no significance, *p<0.05, **p<0.01.*

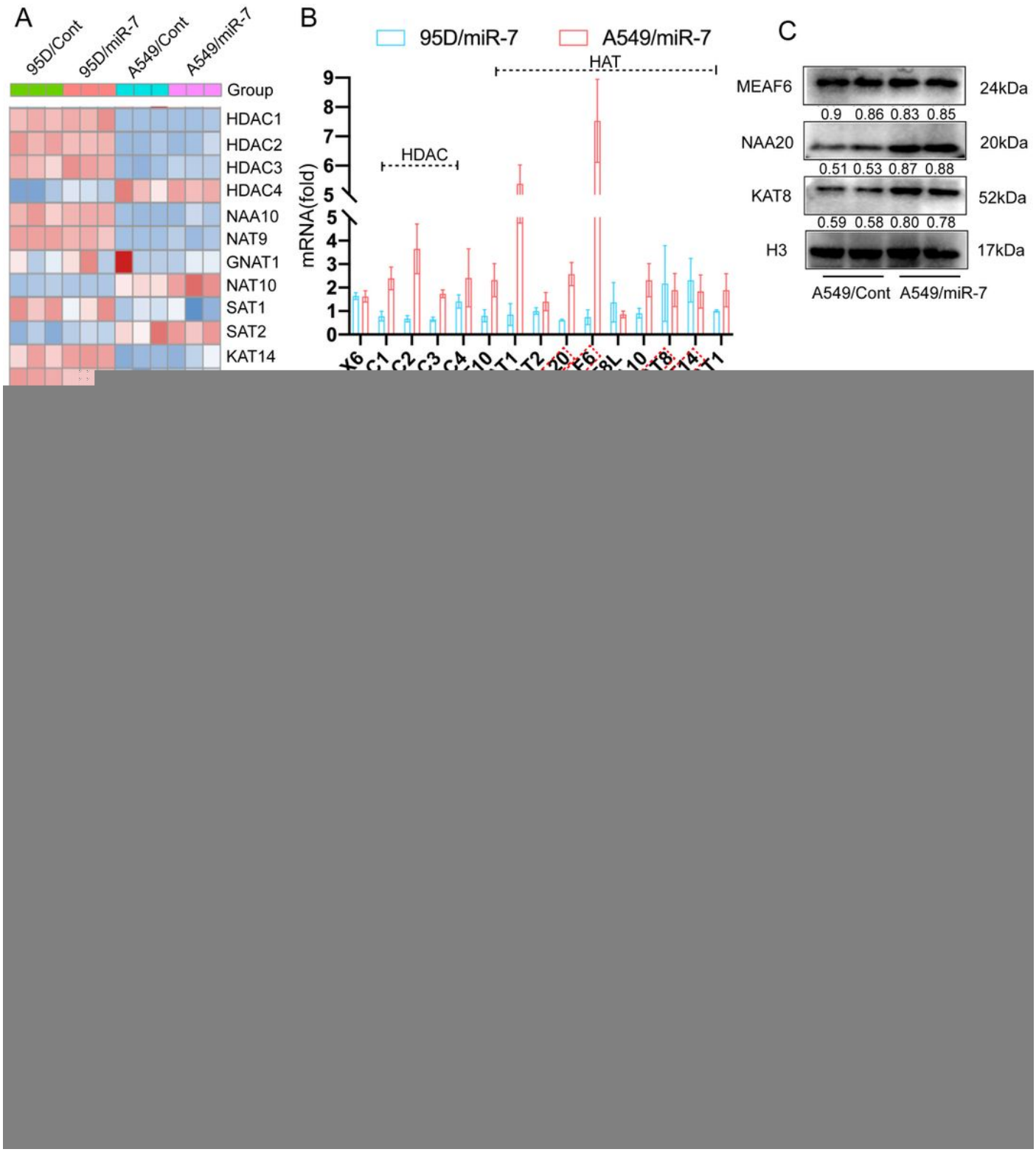

Figure 5

KAT8 regulates PAX6 expression in miR-7-resistant human NSCLC cells.

(A) The expression levels of histone acetyltransferase and histone deacetyltransferase in miR-7-resistant human NSCLC cells and control cells were determined by RNA-seq. **(B)** The expression levels of histone acetyltransferase, histone deacetyltransferase and PAX6 were detected by real-time PCR. **(C)** The

expression levels of MEAF6, NAA20 and KAT8 in A549/miR-7 and A549/Cont cells were detected by western blotting and calculated. **(D)** Human NSCLC cells were transiently transfected with miR-7 (2.5 μg) in 24-well plates using Lipofectamine 3000 reagent *in vitro*, once every two days, three times in total. The expression level of KAT8 in human NSCLC cells was detected by real-time PCR. **(E)** A549/miR-7 cells were transiently transfected with si-KAT8/si-NC (2.5 nM) in 24-well plates using Lipofectamine 3000 reagent *in vitro.* Forty-eight hours later, the expression level of KAT8 was detected by real-time PCR. **(F)** Real-time PCR was performed to detect the expression level of PAX6 in (E). **(G)** The proliferation of (E) was assessed by CCK8 assay. **(H-I)** The expression levels of KAT8 and the PI3K/Akt- and MAPK signaling pathway-related proteins ERK1/2, pERK1/2, PDK1, AKT, p-AKT, and p-PI3K in (E) were detected by western blotting and calculated. Representative data from three independent experiments are shown. *$*p<0.05$, **$**p<0.01$.*

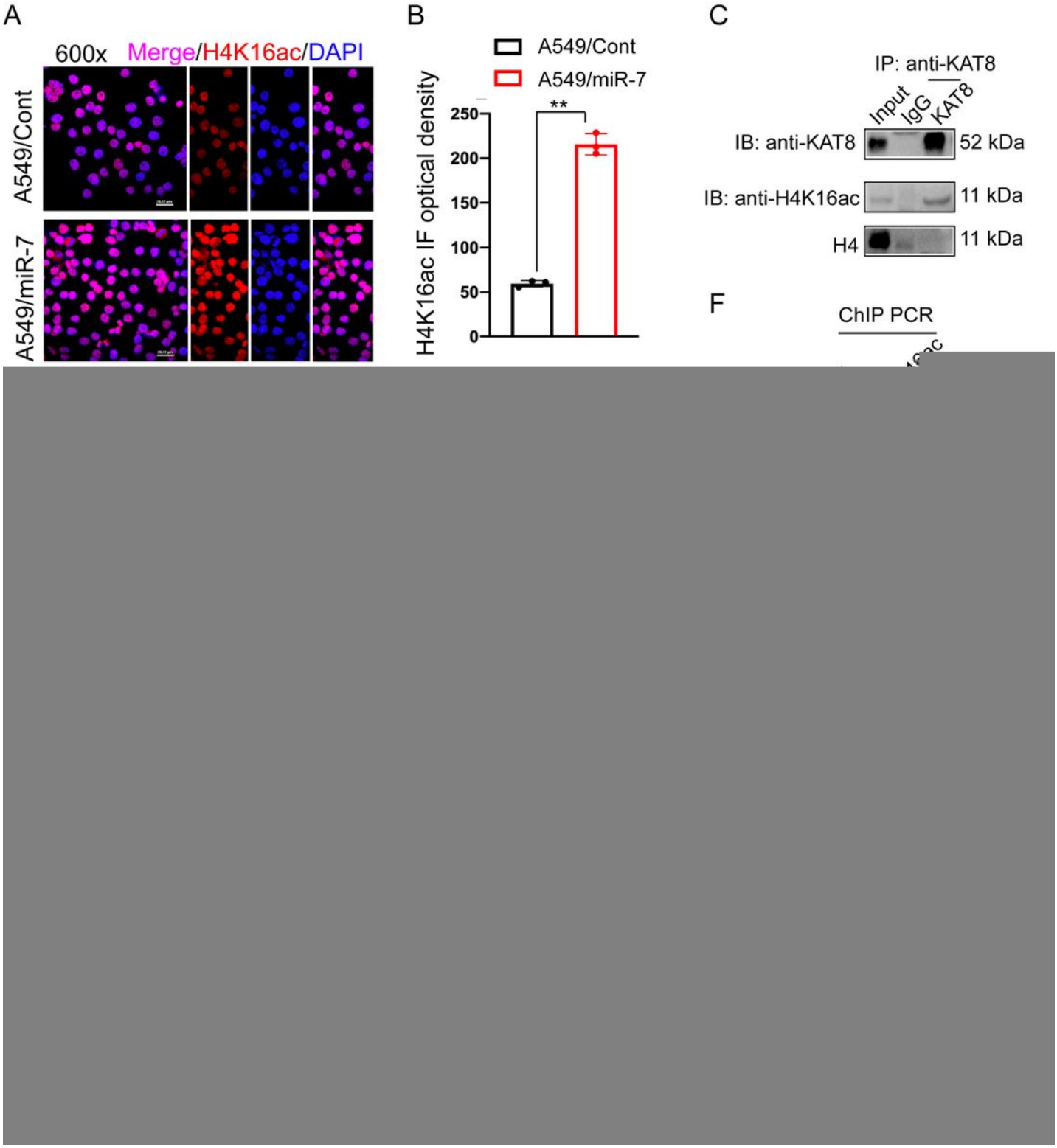

Figure 6

KAT8 regulates PAX6 expression in miR-7-resistant human NSCLC cells *via* H4K16 acetylation.

(A-B) The expression level of H4K16ac was detected by immunofluorescence and quantitated. **(C)** A549/miR-7-cell lysates were incubated with anti-KAT8 to immunoprecipitate and concurrently pull down H4K16ac. **(D-E)** The expression levels of KAT8, H4K16ac and PAX6 in A549/Cont and A549/miR-7 cells

were detected by western blotting and calculated. **(F)** Chromatin immunoprecipitation was used to analyze the binding of H4K16ac to the PAX6 promoter. Input was used as a positive control. **(G)** ChIP–qPCR was performed to confirm the results shown in (F). **(H)** A549/miR-7 cells were transiently transfected with si-KAT8/si-NC (2.5 nM) in 24-well plates using Lipofectamine 3000 reagent *in vitro.* Forty-eight hours later, the protein levels of KAT8, PAX6 and H4K16ac were detected by western blotting and calculated. **(I)** The colocalization of KAT8 and H4K16acand the expression of PAX6 in A549/miR-7 cells were analyzed by immunofluorescence. Representative data from three independent experiments are shown. **p<0.05, **p<0.01.*

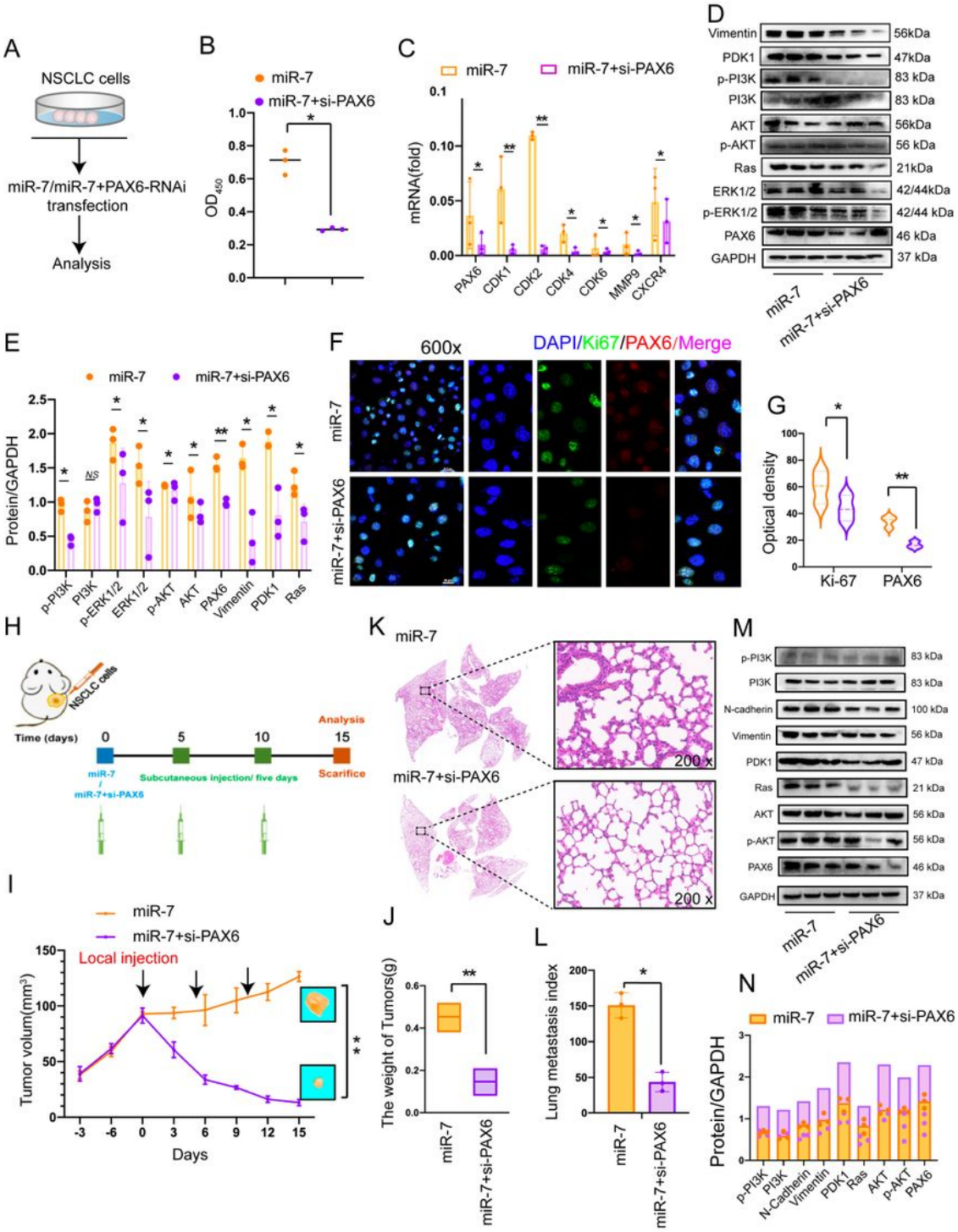

Figure 7

Figure 7

PAX6 silencing improves the inhibitory effect of miR-7 on human NSCLC cells.

(A) Schematic diagram. Human NSCLC A549 cells were transiently transfected with miR-7 (2.5 μg) or miR-7 (2.5 μg) plus PAX6-siRNA (2.5 nM) in 24-well plates using Lipofectamine 3000 reagent. Forty-eight hours later, **(B)** the proliferation of (A) was detected by CCK8 assay. **(C)** The transcription levels of PAX6,

the cell cycle-related CDK1, CDK2, CDK4 and CDK6, and the metastasis-related molecules MMP9 and CXCR4 in (A) were detected by real-time PCR and calculated. **(D-E)** The protein levels of PAX6, the PI3K/Akt- and MAPK pathway-related molecules PDK1, p-PI3K, PI3K, AKT, p-AKT, Ras, ERK1/2, and p-ERK1/2, and the metastasis-related molecule vimentin were detected by western blotting and calculated**.** **(F-G)** The expression levels of Ki-67 and PAX6 were detected by immunofluorescence and quantitated (600×). **(H)** Schematic representation of the *in vivo* experiment. A549 cells (1×10^7) were subcutaneously injected into the right flanks of Balb/c nude mice. Seven days later, the mice were injected with plasmids p-miR-7 (50 μg) or p-miR-7 (50 μg) combined with si-PAX6 (10 nM) every two days for a total of 3 injections. Tumor growth was monitored every three days to generate the growth curve. On day 15, tumor and lung tissues were harvested. **(I)** Tumor growth curve and tumor size. **(J)** Tumor weight. **(K-L)** The representative hematoxylin and eosin-stained tumor tissue in (H) (200×). The metastatic index was calculated. **(M-N)** The expression levels of PAX6, the PI3K/Akt- and MAPK signaling pathway-related proteins PDK1, AKT, p-AKT, PI3K, p-PI3K and Ras, and the metastasis-related proteins N-cadherin and vimentin in tumor tissues were detected by western blotting and calculated. Representative data from three independent experiments are shown. *NS, no significance, * p<0.05, ** p<0.01.*

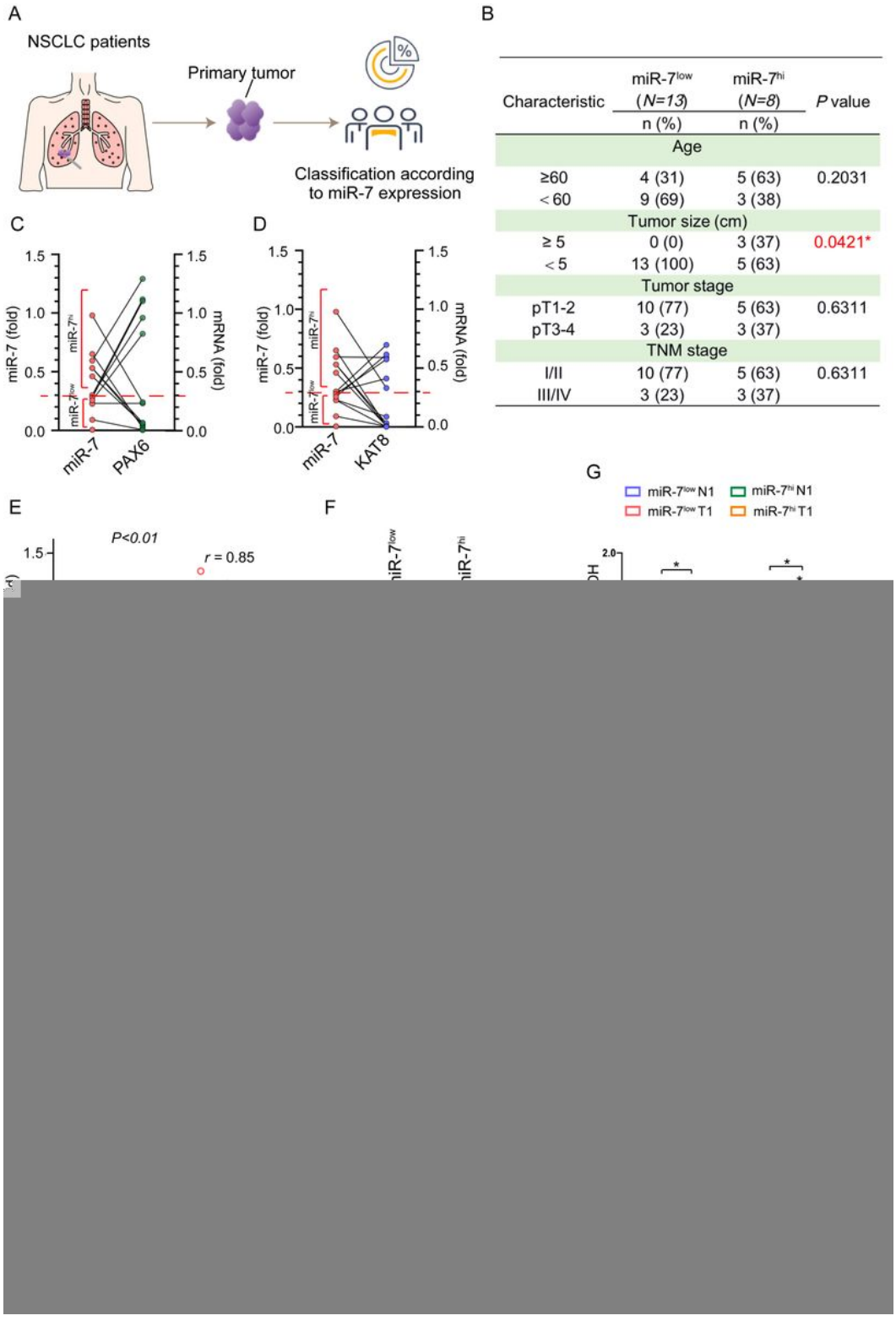

Characteristic	miR-7^{low} (*N=13*) n (%)	miR-7^{hi} (*N=8*) n (%)	*P* value
Age			
≥60	4 (31)	5 (63)	0.2031
< 60	9 (69)	3 (38)	
Tumor size (cm)			
≥ 5	0 (0)	3 (37)	0.0421*
< 5	13 (100)	5 (63)	
Tumor stage			
pT1-2	10 (77)	5 (63)	0.6311
pT3-4	3 (23)	3 (37)	
TNM stage			
I/II	10 (77)	5 (63)	0.6311
III/IV	3 (23)	3 (37)	

Figure 8

The expression levels of miR-7, PAX6 and KAT8 in clinical NSCLC patients and the mechanism by which human NSCLC cells resist miR-7 intervention.

(A) Schematic diagram. The expression level of miR-7 in NSCLC patients was detected by real-time PCR. **(B)** According to the expression level of miR-7 in tumor tissue, the NSCLC patients were divided into two

groups: the miR-7^{high} group (n=8) and the miR-7^{low} group (n=13). Then, the correlations of miR-7 expression and clinicopathological characteristics of NSCLC patients were analyzed (n=21). **(C)** The mRNA levels of miR-7 and PAX6 in each tumor tissue in (B) were determined by real-time PCR and calculated. **(D)** The mRNA levels of miR-7 and KAT8 in each tumor tissue in (B) were detected by real-time PCR and calculated. **(E)** Correlation analysis of KAT8 and PAX6 expression in NSCLC tissues. **(F-G)** The protein levels of KAT8 and PAX6 in NSCLC tissues and matched adjacent noncancerous tissues in both the miR-7^{high} group and miR-7^{low} group were determined by Western blotting and calculated. **(H)** Schematic diagram. Under the condition of miR-7 intervention, human NSCLC cells gain resistance to miR-7 intervention. Importantly, these miR-7-resistant human NSCLC cells exhibit aggressive behavior, including rapid growth and elevated metastasis. Mechanistically, KAT8 regulates PAX6 expression *via* H4K16 acetylation, along with aberrant transduction of the PI3K/Akt pathway, thereby orchestrating the acquired resistance of human NSCLC cells to miR-7 intervention. *$p<0.05$.

Supplementary Files

This is a list of supplementary files associated with this preprint. Click to download.

- SupplementaryMaterials.docx